Two-Dimensional Model of Biofilm Detachment Caused by Internal Stress from Liquid Flow

Cristian Picioreanu,[1,2] Mark C. M. van Loosdrecht,[1] Joseph J. Heijnen[1]

[1]Department of Biochemical Engineering, Delft University of Technology, Julianalaan 67, 2628 BC Delft, The Netherlands; telephone: +31 15 2781618; fax +31 15 2782355; e-mail: Mark.vL@stm.tudelft.nl
[2]Department of Chemical Engineering, University Politehnica of Bucharest, Splaiul Independentei 313, 77206 Bucharest, Romania

Received 24 February 2000; accepted 13 July 2000

Abstract: A two-dimensional model for biofilm growth and detachment was used to evaluate the effect of detachment on biofilm structures. The detachment process is considered to be due to internal stress created by moving liquid past the biofilm. This model generated a variety of realistic biofilm-formation patterns. It was possible to model in a unified way two different biofilm detachment processes, erosion (small-particle loss), and sloughing (large-biomass-particle removal). The distribution of the fraction from total biomass detached as a function of detached particle mass, gives indications about which of the two mechanisms is dominant. Model simulations indicate that erosion makes the biofilm surface smoother. Sloughing, in contrast, leads to an increased biofilm-surface roughness. Faster growing biofilms have a faster detachment rate than slow-growing biofilms, under similar hydrodynamic conditions and biofilm strength. This is in perfect accordance with the experimental evidence showing that detachment is dependent on both shear- and microbial-growth rates. High growth rates trigger instability in biofilm accumulation and abrupt biomass loss (sloughing). Massive sloughing can be avoided by high liquid shear, combined with low biomass growth rates. As the modeling results show, the causes for sloughing must be sought not only in the biofilm strength, but also in its shape. Several "mushroom-like" biofilm structures like those repeatedly reported in the literature occurred, due to a combined effect of nutrient depletion and breaking at the colony base. A rough carrier surface promotes biofilm development in hydrodynamic conditions in which the biofilm on a flat surface would not form. Although biofilm patches filled completely the cavity in which they started to grow, they were unable to spill over the carrier peaks and to fully colonize the substratum. *Biotechnol Bioeng* **72**: 205–218, 2001.
Keywords: biofilm; mathematical model; detachment; erosion; sloughing; shear stress; flow; roughness

INTRODUCTION

Biofilm formation is the result of several physical, chemical, and biological processes occurring simultaneously, including: (1) cell and particle transport to the substratum (also called "carrier" in this study), (2) cell adhesion and attachment, (3) biofilm generation by cellular growth and extracellular polymer production, (4) biofilm detachment, and (5) substrate and product transport to and from the biofilm (Applegate and Bryers, 1990; Bryers and Characklis, 1982).

One-dimensional models including all these processes exist, and they were successfully applied to describe quantitatively substrate conversion in biofilms (Wanner and Gujer, 1986; Wanner and Reichert, 1996). An appropriate description of biofilm-structure formation as the result of environmental factors must be multidimensional, as suggested by Bishop and Rittmann, 1996. First attempts to model biofilm structure included two-dimensional substrate diffusion, reaction and microbial growth (Picioreanu et al., 1998; Wimpenny and Colasanti, 1997). A kind of empirical detachment rule was also implemented in a cellular automaton biofilm model by Hermanowicz (1998). Later, Picioreanu et al. (1999, 2000a, 2000b) incorporated liquid flow past the irregular biofilm surface in their model. The model representation of hydrodynamics, substrate mass transfer and reaction, was then extended to three dimensions by Eberl et al. (1999).

As van Loosdrecht et al. (1995, 1997) suggested, biofilm detachment is a determining factor for biofilm-structure formation, because it is the primary process that balances growth. Detachment of large biofilm aggregates will generally create a very irregular biofilm–liquid interface. Therefore, it plays a role in development of biofilm spatial heterogeneity ("patchiness;" Stewart, 1993). A rough biofilm surface could create favorable niches for bacterial attachment and secondary colonization. This might lead to introduction of new microbial species into the biofilm. If a considerable part of the biomass has been removed, more substrate becomes available for the remaining cells. It was also recognized that detachment greatly affects performance and stability of biofilm reactors, because practical biofilms exhibit fluctuations in thickness and surface geometry (Tijhuis et al., 1996).

Despite all evidence about its importance, a quantitative

Correspondence to: M. van Loosdrecht
Contract grant sponsor: The Netherlands Organisation for Applied Scientific Research (TNO)
Contract grant number: 95/638/MEP

model description of the influence of the detachment process on biofilm heterogeneity is still missing. One difficult point for the modeler is that detachment is said to be due to at least four different mechanisms (Bryers, 1988): erosion, sloughing, abrasion, and predator grazing. Erosion is the continuous removal of small particles from the surface of the biofilm (Rittmann, 1989). Sloughing is seen more as a discrete process, consisting in loss of large patches of biofilm. Generally, it is assumed that these biomass-loss processes are caused by different factors. Stewart (1993) remarked that distinction between erosion and sloughing may be arbitrary, because in many systems there is a broad distribution of detached particle sizes. Therefore, a unified approach to erosion and sloughing seems to be justified.

Causes for erosion and sloughing reside both in forces created by a moving fluid past the biofilm, and in the biofilm structure itself. Thus, a quantitative model describing detachment at microscopic scale must include calculation of shear and normal forces caused by the flow. This can be a difficult problem because of the very irregular nature of the biofilm–liquid interface. However, calculations are possible, and a biofilm model including flow has already been created by Picioreanu et al. (1999, 2000b) and Eberl et al. (1999) The one uncertainty remaining is the quantification of biofilm internal factors determining detachment. Work done by Ohashi and Harada (1994, 1996) and Ohashi et al. (1999) revealed the possibility of measuring the biofilm mechanical strength. They found that biofilm strength increased with an increasing dry density. The decay of cells in the biofilm depth due to aging or starvation, leads to a decrease of the adhesive strength. Mechanical properties indispensable for a biofilm-detachment model caused by internal stress are the elastic modulus and the Poisson ratio. Values of these properties were reported by Christensen and Characklis (1990) and Stoodley et al. (1999a).

Given both the state of experimental research in the biofilm field, and the computing power existing nowadays, our goal is to show that it is possible to create a model, explaining in a deterministic way, the heterogeneous structure of biofilms created by the interplay of growth and detachment processes caused by fluid-flow-induced stress. In this article, the frame of such a model will be proposed, and first results of model simulations will be analyzed. We do not intend to present a model that fully incorporates all processes of relevance for biofilm formation. We only included those processes for which sufficient mechanistic foundation is available. This still allows evaluating how biofilm detachment influences the biofilm structures, without including predetermined effects in the model itself.

MODEL DESCRIPTION

Model Formulation and General Assumptions

The geometry of the model system used and the boundary conditions are the same as in Picioreanu et al. (2000b). The model aims to simulate biofilm formation and detachment in a system similar to a flow-cell. Water flows between two parallel plates, transporting the nutrients on which bacterial films grow. The liquid flow-rate is kept constant in time. Flow, mass transport, and growth processes included in this model were described in previous articles (Picioreanu et al., 1998, 1999, 2000b). Therefore, in this study we will focus mainly on the detachment mechanisms.

We assume that biofilm detachment results from the combined effect of liquid shear and biofilm strength. Experimental evidence has shown that the detachment rate is strongly dependent on the hydrodynamic regime in the reactor (Rittmann, 1982). The liquid flow above the biofilm exerts forces on the biofilm structure, both in normal and tangential direction to its surface. These forces cause tensile and shear loads that the gel structure must support in order not to break. Flow calculations must therefore be performed prior to detachment, to provide the normal (σ_X^w, σ_Y^w) and tangential (τ_{YX}^w) components of the liquid stresses at the biofilm surface. The consequence of these applied forces is a state of stress acting on the biofilm structure. To determine the places where the material will break due to a too high internal stress, a finite element analysis was performed. The following assumptions have been made:

1. The biofilm body is approximated as an *elastic material* (Ohashi et al., 1999).
2. The biofilm is *homogeneous and isotropic*. There is no variation of elastic coefficient *E,* Poisson ratio ν_p and tensile strength σ_t with cell or EPS content of the biofilm. Ohashi et al. (1999) found a dependence between σ_t and the cell density in the biofilm, but this is still not quantifiable.
3. Small displacements in the elastic limit do not influence the liquid flow. This means that, although the biofilm deforms, the flow profile is solved taking only the nondeformed biofilm geometry.
4. *No vibrations* caused by the flow occur in the biofilm. Oscillating biofilm streamers analyzed by Stoodley et al. (1998) were much longer (up to 3 mm) than biofilm filaments resulted from our model (maximum 150 μm). Moreover, liquid velocities in our system were smaller than in Stoodley's study, and they would probably be unable to trigger significant vibrations. Still, oscillations of biofilm filaments might have an important effect on drag and on mass transfer.
5. The fully three-dimensional situation is reduced to a two-dimensional problem by assuming all surface forces acting only in the xy plane (i.e., have no z component). The normal strain in the z direction is zero, implying a biofilm in the *state of plane strain.* The only surface stresses are σ_X^w, σ_Y^w, and τ_{YX}^w resulting from the two-dimensional flow pattern.
6. We assume that broken biofilm patches are quickly taken away by the flow and washed-out from the system. *Reattachment is not possible* in this model. The flag of any grid cell that contained detached biomass

will be switched to contain liquid after detachment. "Islands" of biomass, which have lost the solid connection with the biofilm, are also removed.
7. There are *no other stress sources* in the biofilm volume (as, for example, bacterial growth in a gel matrix can generate).
8. The biofilm is considered a *ductile material*, which exhibits "yielding" followed by some plastic deformation prior to fracture. This was shown by experiments of Ohashi and Harada (1994).
9. The *biofilm-carrier interface* is characterized by rigid but breakable bonds. For simplicity, the biofilm internal strength (called "cohesion strength" in this study) and the adhesion strength at the biofilm-carrier interface are considered the same.
10. *Biofilm failure* occurs according to the maximum-distortion-energy theory (see any textbook on the mechanics of elastic materials, e.g., Benham et al., 1996; Hibbeler, 1991).

Model Equations

Liquid flow in the laminar regime is governed by the incompressible Navier-Stokes equations. The substrate mass balance includes convective- and diffusive-transport terms for the liquid domain, and diffusion plus reaction in the biofilm volume. All equations for flow, mass transport and growth processes, together with the initial and boundary conditions, were presented in Picioreanu et al. (1999, 2000a, 2000b).

For stress calculation in structures, the governing equations for mechanical equilibrium and compatibility (Benham et al., 1996) must satisfy the boundary conditions of the plane strain problem as defined by the applied liquid forces. These equations, presented in the Appendix, are solved to yield first the components of the strain tensor (ϵ_X, ϵ_Y, γ_{YX}) and then the stresses (σ_X, σ_Y, τ_{YX}) at required points in the structure. As boundary conditions, the normal and shear stresses on the biofilm surface must be specified. Zero-displacement condition is set on the biofilm-carrier interface.

To determine where failure will occur, the maximum-distortion-energy criterion will be applied in each element. A material, when deformed by external loading, tends to store energy internally throughout its volume. Three- or two-dimensional yielding in a ductile material occurs when the distortion energy per unit volume of the material (U_d), exceeds U_d of the same material when subjected to yielding in a simple (one-dimensional) tension test (Hibbeler, 1991). In terms of normal (σ_X and σ_Y) and shear (τ_{YX}) stresses, the failure criterion in two-dimensional state of strain reads:

$$\sigma_X^2 - \sigma_X \sigma_Y + \sigma_Y^2 + 3\tau_{YX}^2 = \sigma_e^2 > \sigma_t^2 \qquad (1)$$

meaning that fracture occurs when the equivalent stress, σ_e is larger than the ultimate tensile stress before fracture, σ_t (see, for example, Benham et al., 1996; Hibbeler, 1991). In this work, biofilm breakage was considered to occur when σ_e is greater than the cohesion strength. Cohesion strength can be understood (Ohashi et al., 1994) as the biofilm internal force per unit area that is resistant to the tensile stress just before detachment.

Model Parameters

The model needs biological parameters (microbial growth rates, stoechiometric yields, saturation constants, and maintenance coefficients), physical properties of the liquid phase (viscosity, density) as well as of the dissolved components (diffusion coefficients). These parameters are, in general, widely available from literature, as given in Table I.

The detachment model additionally requires knowledge about some mechanical properties of biofilms, such as the elastic (Young) modulus, E, Poisson ratio, ν_P, and cohesion strength, σ_t. About these properties, there is only very scarce information in the literature. Christensen and Characklis (1990) reported a biofilm elastic modulus of about 60 N/m^2. Stoodley et al. (1999a) found values of E on the same order of magnitude, in the range of 10 to 240 N/m^2. Cohesion strength of denitrifying biofilms was measured by Ohashi et al. (1994). After 32 days of biofilm growth, they found cohesion strengths in the order of σ_t = 10 N/m^2 near the carrier interface, varying to 0.1 N/m^2 in the vicinity of the outer surface. Tendencies of σ_t to increase with progression of biofilm formation and with biofilm dry density were also observed. In this study, we took values of σ_t between 0.4 and 1 N/m^2, E = 64 N/m^2 and ν_P = 0.3 (Table I).

Simulation Plan

Three characteristic parameters for the system studied were varied: the G ratio, Re number and the biofilm cohesion strength σ_t. The effect of internal substrate transfer rate on biofilm growth is incorporated in the G ratio, as defined in Picioreanu et al. (1998):

$$G = \frac{\text{maximum biomass growth rate}}{\text{maximum substrate transport rate}} \qquad (2)$$

G is obtained by multiplying the Thiele modulus ϕ^2 by the biomass growth yield on substrate, Y_{XS}. A high value of G means mass-transfer limitation, while a lower one means a limitation of biofilm development by microbial growth rate. Practically, these regimes were realized in the model by setting the substrate concentration in the inlet at low (c_{S0} = 0.4 g m^{-3}), and at high (c_{S0} = 8 g m^{-3}) values, respectively. The Re number was defined based on the flow-channel total width (1000 μm) and average liquid velocity in inlet, $u_0 = 2/3 \cdot u_{Xmax}$. Simulations at G = 562 and 28, Re = 6.7 and 13.3, and σ_t = 0.4, and 1 Nm^{-2} were performed.

Algorithm

The general algorithm used is similar to that presented in detail in Picioreanu et al. (2000b), but it now also incorpo-

Table I. Model parameters.

Model parameter	Symbol	Parameter value	Units
Physical properties			
Oxygen diffusion coefficient	D_s	$2.3 \cdot 10^{-9}$	$m^2\ s^{-1}$
Liquid kinematic viscosity	ν	10^{-6}	$m^2\ s^{-1}$
Liquid density	ρ	1000	$kg\ m^{-3}$
Biomass properties			
Maximum biofilm biomass density	c_{Xm}	30	$kg_X\ m^{-3}$
Biomass maximum specific growth rate	μ_m	$1.5 \cdot 10^{-5}$	s^{-1}
Oxygen saturation constant	K_S	$3.5 \cdot 10^{-4}$	$kg_S\ m^{-3}$
Biomass yield on substrate	Y_{XS}	0.045	$kg_x\ kg_S^1$
Maintenance coefficient	m_S	$3 \cdot 10^{-5}$	$kg_S\ kg_X^{-1}\ s^{-1}$
Biofilm mechanical properties			
Elastic (Young) modulus	E	64	$N\ m^{-2}$
Poisson ratio	ν_P	0.3	—
Cohesion strength	σ_t	0.4 and 1	$N\ m^{-2}$
System properties			
Physical system dimensions	$L_X \times L_Y$	1000 × 500	μm
Computational grid dimensions	$N_X \times N_Y$	256 × 129	grid nodes
Maximum velocity in inlet flow	$u_{X,max}$	10^{-2} and $2 \cdot 10^{-2}$	$m\ s^{-1}$
Number of grid elements inoculated with biomass	n_0	15 and 60	—
Bulk oxygen concentration	c_{S0}	$0.4 \cdot 10^{-3}$ and $8 \cdot 10^{-3}$	$kg_S\ m^{-3}$

rates the detachment mechanism. Time-scale separation is assumed, so that we solve only one biofilm process at a time. The detachment process is executed after solving the flow pattern, because it requires as input the values of wall shear stresses σ_X^w, σ_Y^w, and τ_{YX}^w. After a biofilm breaking event, boundaries of the system change and the flow field must be recalculated. The sequence: flow calculations, stress calculations, and detachment will be repeated until no further detachment takes place. Because we assume the breaking process as being very fast (having the characteristic time in the same order of magnitude as momentum transfer), the mass-transfer step is executed only when a mechanical equilibrium (i.e., no detachment) is reached. The solution of the steady-state substrate mass balance, c_S, is further used in the biomass growth kinetics to calculate biomass concentration, c_X, in each grid element. Biomass will be then redistributed from each grid cell where c_X exceeded a critical value, c_{Xm}, according to the discrete algorithm used in Picioreanu et al. (1998). If the biofilm surface has changed after biomass spreading, the flow field is recalculated and the whole computational cycle is repeated. The algorithm steps are summarized below:

1. Hydrodynamic step: computes the flow variables pressure p, velocity u, stress σ^w.
2. Stress step: computes the equivalent stress σ_e in the biofilm structure
3. Detachment step: turn into liquid state every biofilm volume element where ($\sigma_e > \sigma_t$)
   - If biofilm geometry has changed, then go to step 1.
4. Mass transfer step: computes the substrate concentration c_S.
5. Growth step: computes the biomass concentration c_X.
6. Spreading step: redistribute the biomass from all elements having $c_X > c_{Xm}$
   - If biofilm geometry has changed, then go to step 1.

Model Solution

Flow and mass transfer equations were solved with a nine-speed lattice Boltzmann method (see e.g., Chen et al., 1995), by using the algorithm described and tested in Picioreanu (1999). The lattice Boltzmann method has the advantage of easily handling irregular geometries, like the biofilm surface is in our case. In addition, it is very suitable for parallelization, a very desirable feature in long and complex computations.

A finite-element method was used to solve the plane-strain problem and to find the principal stresses in the biofilm structure. The type of finite element used was the parabolic isoparametric element. The basis of the method, a general algorithm and program code were described in a textbook by Hinton and Owen (1977).

RESULTS AND DISCUSSION

Wall Shear Stress

Because the stresses generated by the liquid flow at the biofilm surface constitute the boundary condition for the equations of mechanical equilibrium in the biofilm, their correct computation is essential. We have shown in Picioreanu (1999) that the lattice Boltzmann method can provide values of wall shear stress accurate enough for the purpose of our model.

Internal Stress Field

Analysis of stress accumulation is important because it determines the places in the structure where fracture most probably will occur. An example of equivalent stress distribution in the biofilm structure is shown in Figure 1. A few typical situations when the biofilm breaks were identified:

1. In compact biofilm clusters (like the hemispherical one in Fig. 1d), the highest stress develops near the biofilm surface. This is especially caused by the shear component of stress. Biofilm erosion, defined as continuous loss of small amounts of biomass from the biofilm surface, can be the result of these stresses.
2. In finger-like clusters the stress also builds up near the biofilm-carrier interface, due to a high bending momentum. "Necks" especially concentrate stress (Fig. 1a–d). In general, cracks form in the narrowest part (the smallest cross-sectional area) of the biofilm filaments. This leads to breakage of a whole biofilm patch, a phenomenon known as "sloughing."
3. Isolated colonies or simply the first one that faces the flow are less protected from the shearing effect of flow. Although it grows faster than other colonies, because it receives more substrate (Picioreanu et al., 2000b), stress builds up easier in the first structure from the left in Fig. 1b. Consequently, these colonies will also be eroded and sheared off at a higher rate. This coincides with experimental observations by Gjaltema et al. (1994), who reported that sloughing always started at the upstream side of the slides in a RotoTorque bioreactor.

These findings are in agreement with the experimental results of Ohashi and Harada (1994), showing that convex parts of the biofilm surface were more subject to detachment than concave parts.

Biofilm Evolution in Time

Very similar to the sigmoidal fashion of biofilm development presented by Bryers and Characklis (1982), four phases can be clearly distinguished in the evolution of simulated biomass amount per carrier area, ρ_X ($g_X m^{-2}_{carrier}$). In the initial phase, there is no substrate limitation because the biofilm is thin, and microbial growth occurs in the whole biofilm at rates close to the maximum. The biomass amount per carrier area follows an exponential growth curve (phase I, Fig. 2a–f). There is frequently a lag phase, as seen in Fig. 2c. When the biofilm becomes thicker, there is substrate limitation in deeper biofilm layers. Growth is possible only in an active layer close to the biofilm–liquid interface. In this mass-transfer-limited regime, the biomass amount grows linearly (phase II), being produced only in a layer of almost constant thickness. In a third phase, the growth rate of the total biomass per carrier area slows down, because biomass decays in layers below the substrate penetration depth. In all these phases, biofilm growth is balanced only by superficial erosion. When a certain thickness is achieved, the biofilm enters a new phase. It is now exposed to sloughing, where bigger biofilm patches are detaching. In the following, we will define t_S as being the time at which the first major sloughing event occurs, $\rho_{X,S}$ is the corresponding biomass per carrier area at t_S, and $\bar{\rho}_X$ is the biomass per carrier area averaged over the whole sloughing period simulated (Fig. 2b). Figure 2 shows, together with the biomass amount accumulated on the carrier (curves marked with

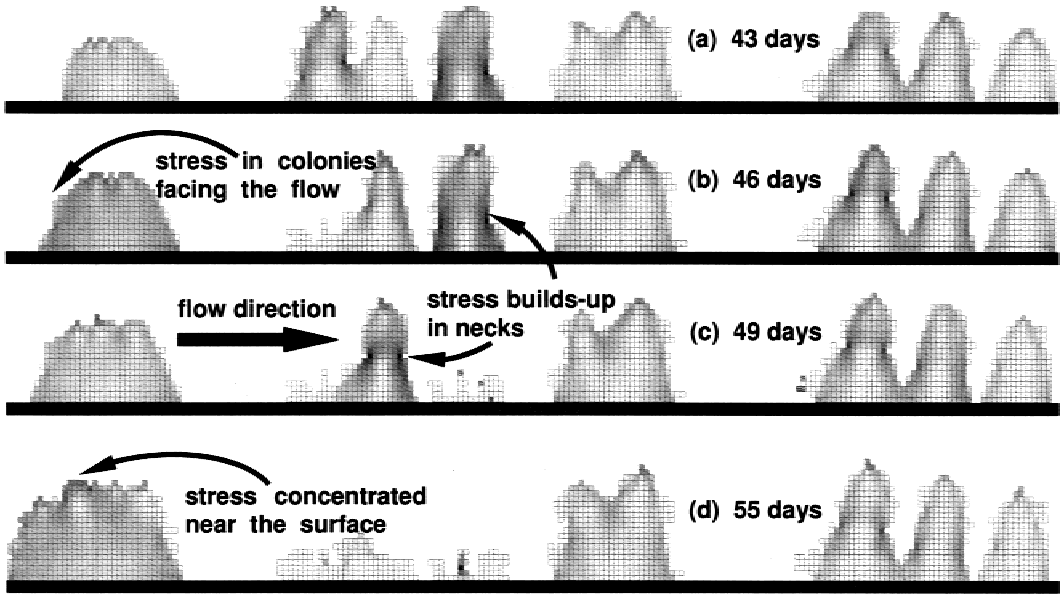

Figure 1. Distribution of mechanical stress in some simulated biofilm structures. In each of the four configurations, the equivalent stress, σ_e, was normalized relative to the maximum value existing at that moment in the structure. On the gray scale, black represent finite elements where σ_e is maximum, and white where it is minimum. The stress fields presented correspond to the simulation (b) in Table II (G = 562, Re = 6.7 and σ_t = 1 N m^{-2}).

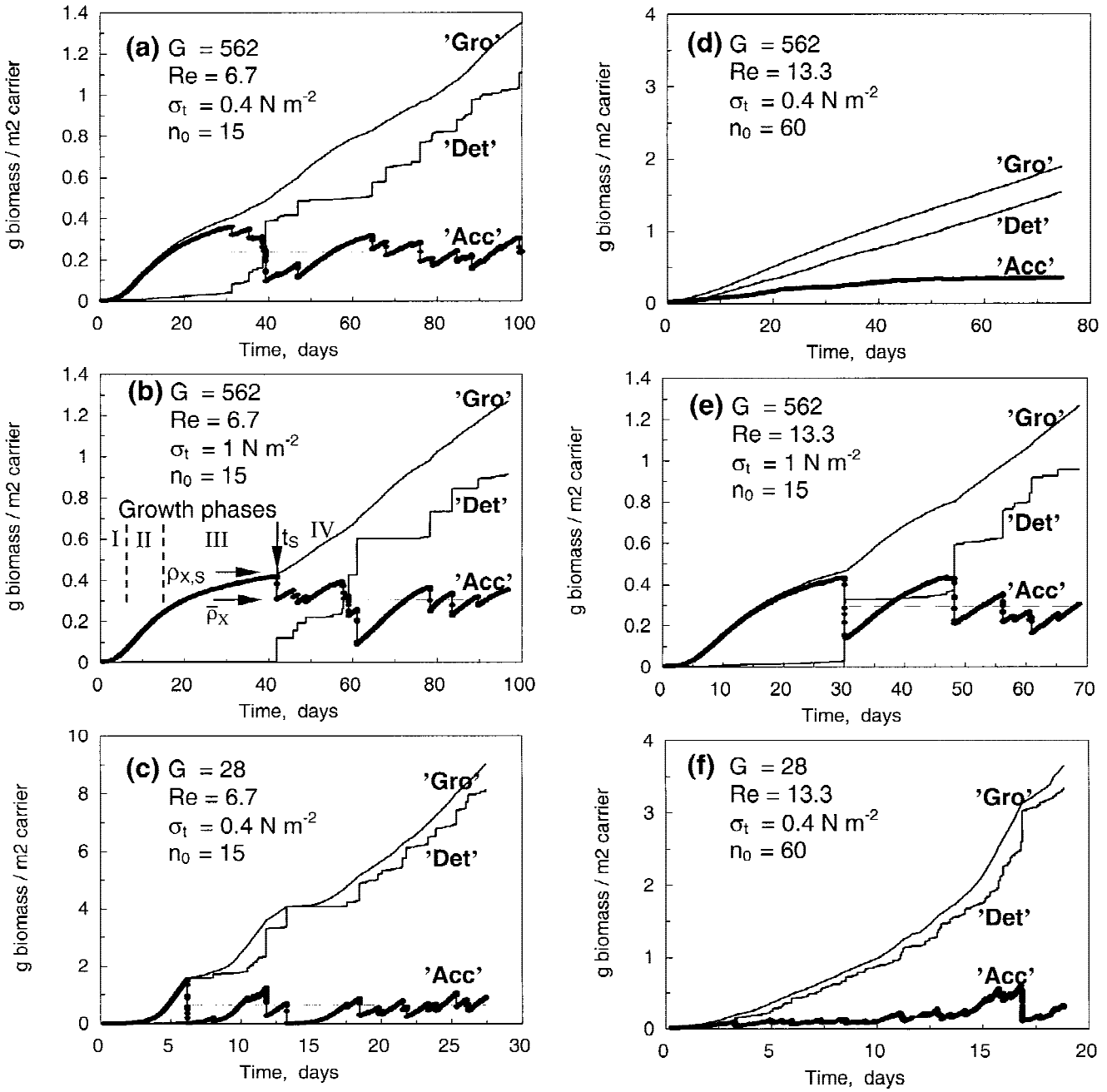

Figure 2. Evolution in time of newly grown biomass ('Gro'), detached ('Det'), and accumulated per unit area of carrier ('Acc'). Parameters in graphs (a)–(f) correspond to those in Table II, cases (a)–(f), respectively. (b) Biofilm growth phases: I—exponential, II—linear, III—decay, IV—sloughing. Dashed lines indicate the biomass amount accumulated on carrier unit area, $\bar{\rho}_X$, averaged over the sloughing period IV.

'Acc'), the biomass newly grown (curves 'Gro') and biomass detached (curves 'Det'). Because the biomass accumulated in the biofilm (ρ_X) is the net result of growth and detachment, it can be expressed as the difference $\rho_X = \rho_{X,g} - \rho_{X,d}$. Before t_S, detachment is caused by erosion only. The average biofilm erosion rate, $\overline{\Phi}_{X,e}$, can be calculated as

$$\overline{\Phi}_{X,e} = \frac{\rho_{X,d}(t_S) - \rho_{X,d}(t=0)}{t_S} \tag{3}$$

where $\rho_{X,d}$ is the amount of biomass detached per unit of carrier area. Similarly, an average biofilm detachment rate for the sloughing period, $\overline{\Phi}_{X,d}$, can be defined between t_S and the end of simulation. In addition, average biomass growth rates $\overline{\Phi}_{X,g}$ were in the same way defined for the biofilm presloughing and sloughing phases. Computed values of these rates in different simulation conditions are presented in Table II.

At high G ratio (G = 526, c_{S0} = 0.4 g/m^3), big breaking events started in the decay phase (Fig. 2a,b,e). In a simulation at low G ratio (G = 28, c_{S0} = 8 g/m^3, Fig. 2c,f) the

Table II. Simulation results.

Variable	Units	Simulation case					
		a	b	c	d	e	f
G ratio	—	562	562	28	562	562	28
Re number	—	6.7	6.7	6.7	13.3	13.3	13.3
Cohesion strength, σ_t	$N\ m^{-2}$	0.4	1.0	0.4	0.4	1.0	0.4
Grid elements inoculated	—	15	15	15	60	15	60
Substrate concentration, c_{S0}	$g\ m^{-3}$	0.4	0.4	8.0	0.4	0.4	8.0
Liquid velocity, $u_{X,max}$	$m\ s^{-1}$	0.01	0.01	0.01	0.02	0.02	0.02
Time of first sloughing, t_S	Days	31.3	42.0	6.2	no	30.0	16.5
Time interval used in averaging before the first sloughing event	Days	0–30	0–41	0–6	0–40	0–30	0–10
Avg. detachment rate, $\overline{\Phi}_{X,d}$	$g_X m^{-2}\ d^{-1}$	0.0014	0.0002	0.0380	0.0190	0.0010	0.0898
Avg. growth rate, $\overline{\Phi}_{X,g}$	$g_X m^{-2}\ d^{-1}$	0.0130	0.0103	0.1650	0.0260	0.0156	0.0993
Substrate flux at t_S, $\overline{\Phi}_{S,C}$ (t_S)	$g_S m^{-2}\ d^{-1}$	1.10	1.15	20.60	1.32	1.32	16.50
Biofilm thickness at t_S	μm	60	106	133	no	78	63
Biomass at t_S, $\rho_{X,S}$	$g\ m^{-2}$	0.363	0.422	1.548	no	0.435	0.620
Time interval used in averaging during the sloughing phase	Days	31–100	42–100	7–27	60–78	31–100	10–17
Avg. detachment rate, $\overline{\Phi}_{X,d}$	$g_X m^{-2}\ d^{-1}$	0.015	0.014	0.310	0.024	0.017	0.230
Avg. growth rate, $\overline{\Phi}_{X,g}$	$g_X m^{-2}\ d^{-1}$	0.014	0.015	0.340	0.025	0.021	0.320
Avg. substrate flux, $\overline{\Phi}_{S,C}$	$g_S m^{-2}\ d^{-1}$	0.92	1.06	11.57	1.37	1.14	no
Avg. biofilm thickness, $\overline{\delta}_f$	μm	55	75	102	25	65	no
Avg. biomass, $\overline{\rho}_x$	$g_X\ m^{-2}$	0.240	0.301	0.656	0.346	0.295	no
Avg. roughness	—	0.45	0.52	0.43	0.16	0.54	no

sloughing began earlier, during the linear biofilm growth (second phase). After that, strong fluctuations occurred in the amount of biomass accumulated on the carrier. Sloughing is represented by steep jumps up on the detachment curves, while erosion is characterized by a gradual increase in the amount of biomass detached. As can be seen from the detachment curves $\rho_{X,d}(t)$ (curves **'Det'** in Fig. 2a,c,e), the sloughing mechanism is clearly responsible for the major biomass loss, although erosion is still present. However, at low substrate concentration (Fig. 2d; G = 526, Re = 13.3, and $\sigma_t = 0.4\ N/m^{-2}$), no sudden biomass loss was observed. In this last case, the biomass reached a stable steady state. Biomass growth rate was balanced and a detachment rate was caused by erosion only.

In many cases, an "avalanche" effect was observed in biomass loss—as seen in Figure 2b between days 40 and 60, for example. This phenomenon can be easily understood by analyzing the biofilm structures shown in Figure 3. In the initial phases of biofilm formation, growth is counteracted only by superficial erosion (days 1–42). After the biofilm reached a certain maturity, a crack appears in the cell cluster most exposed to fluid forces (first from the left). The crack propagates through the structure, and finally, most of the colony fails under a stress exceeding its cohesion strength. After its detachment, the next cluster receives the flow impact, and due to the stress build-up in the neck zone, it breaks. The concentration of mechanical stress at four moments is shown in Figure 1a–d. Other two neighboring finger-like clusters break consecutively between day 46 and day 49, then followed by those shown in the right side of the picture (at days 55–60). By now, the remaining biofilm is thin enough to resist the shearing effect of the fluid. Its growth will continue without major biomass loss for another 2 weeks (until day 76). Then, a new sequence of sloughing events will occur. Also noticeable is the appearance of a "mushroom-like" colony at day 86.

After undergoing a dramatic sloughing event, the biofilm starts growing again from the few colonies left attached to the carrier. The biomass amount accumulated just before the first major sloughing event is never reached again. This is, in our model, probably due to the fact that after a large biomass wash-out, only a few unevenly distributed colonies are left on the carrier surface (see for example the biofilm formation presented in Fig. 4, at day 7 and at day 14). A large carrier surface remains uncovered, which probably does not happen in reality. In our current model a reattachment mechanism is not present, which causes the bare carrier after sloughing; this does not influence the general trends in the observations described in this article. Continuous attachment and reattachment processes, driven probably by the liquid flow, must be introduced in a future, more refined, model. However, it is essential that first, more reliable experimental research on the exact mechanisms be carried out.

The evolution of two simulated biofilms, both grown at G = 562 and $\sigma_t = 0.4\ N/m^2$, is shown in Figure 5. The difference between these biofilms consists in the flow regime in which they were formed. The simulation presented in Figure 5a–e was carried out at Re = 13.3 (starting with 60 grid elements inoculated), while that in Figure 5f–j was done at Re = 6.7 (with biomass distributed initially in 15 grid elements). It is remarkable that the combined effect of

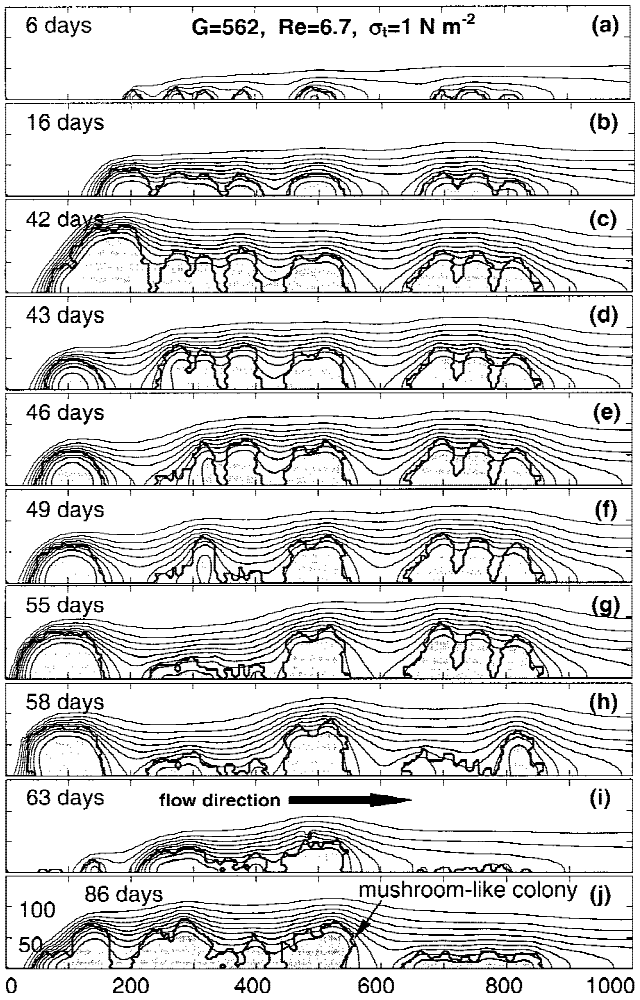

Figure 3. Simulation of biofilm development at G = 562, Re = 6.7, and σ_t = 1 N m^{-2} (Table II, case b). Thick contour lines indicate the biofilm–liquid interface. Substrate concentration field is shown both with iso-concentration lines and with patches on a gray scale. There is 10% variation in concentration between lines. White means maximum concentration in bulk liquid. All graphs have the same scale of 1000 × 150 μm. Flow direction is from left to right.

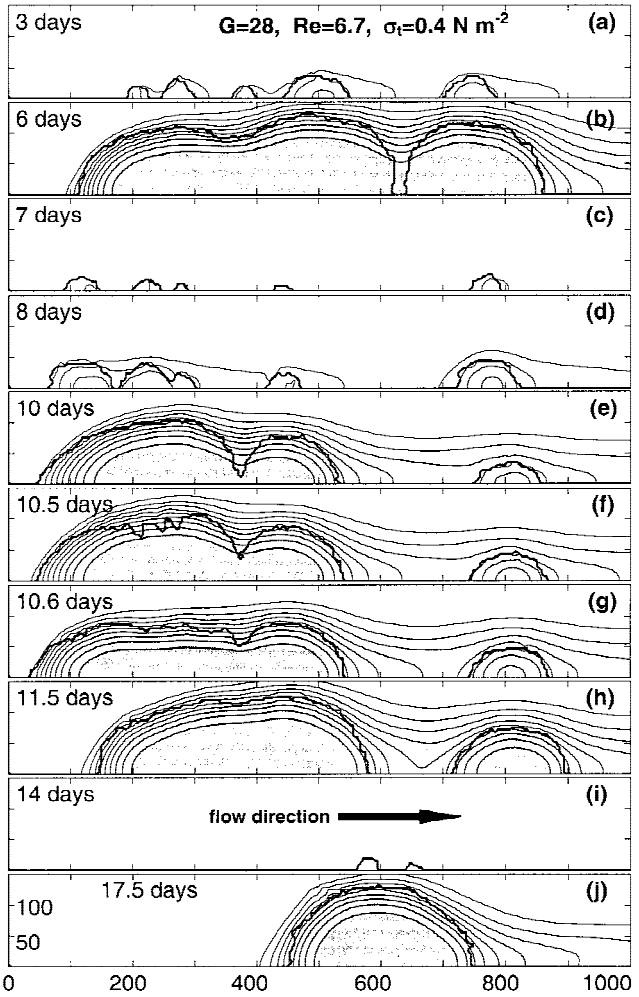

Figure 4. Simulation of biofilm development at G = 28, Re = 6.7 and σ_t = 0.4 N m^{-2} (case c in Table II). Signification of lines and gray scale is as described in Figure 3. All graphs have the same scale of 1000 × 150 μm.

high shear stress and dense inoculation produced a compact biofilm. Although this biofilm is thin, its compactness ensures a high mechanical stability, a very good coverage of carrier surface, a constant level of the biomass accumulated (see Fig. 2d), and consequently, a stable substrate-uptake rate (shown in Fig. 6, where the two lines correspond to the biofilm structures from Fig. 5). Presumably, this is the type of biofilm desirable in wastewater-treatment bioreactors. In contrast, the structure shown in Figure 5f–j evolves as a patchy biofilm. No sloughing occurs in the first 30 days, but in the following 10 days all the clusters break one by one. However, it should be mentioned that the length of our biofilm-model system was rather small, due to obvious computer limitations. This is why the evolution of the averaged biofilm properties suffered abrupt changes, which would be much smoother if averaged on longer carrier length.

Effect of G Ratio, Re Number, and Cohesion Strength on Biofilm Development

G Ratio

The influence of G ratio can be seen in Table II, by comparing simulation cases (a) with (c) (at lower fluid velocity), or (d) with (f) (at the higher liquid velocity). An increase in bulk substrate concentration (low G) leads to a greater substrate flux into the biofilm. The biofilm-growth rate increases, and consequently, the detachment rate is also bigger. In addition, the biomass amount detached relative to that newly formed was bigger. In the erosion stage before sloughing, $\overline{\Phi}_{X,d}$ was 10% from $\overline{\Phi}_{X,g}$ at Re = 6.7 and G = 562, and 20% at G = 28 (Table II). When Re increases to 13.3, erosion becomes really important: 75% of the biomass-growth rate is balanced by the detachment rate at G = 562 and 90% at G = 28. In the sloughing stage, the average detachment rate equals the average growth rate, giving a dynamic equilibrium of biofilm formation on the carrier. A much higher detachment in growing conditions than in non-

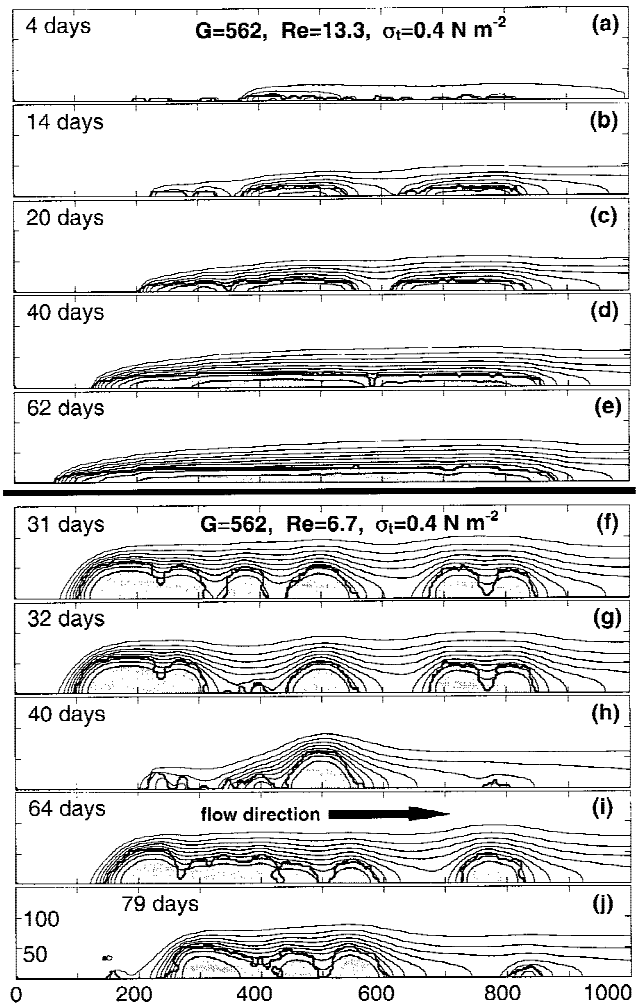

Figure 5. Simulation of biofilm development in two cases at: (a)–(e) G = 562, Re = 13.3, and σ_t = 0.4 N m^{-2} (case d in Table II), (f)–(j) G = 562, Re = 6.7, and σ_t = 0.4 N m^{-2} (case a in Table II). Signification of lines and gray scale is as described in Figure 3. All graphs have the same scale of 1000 × 150 μm.

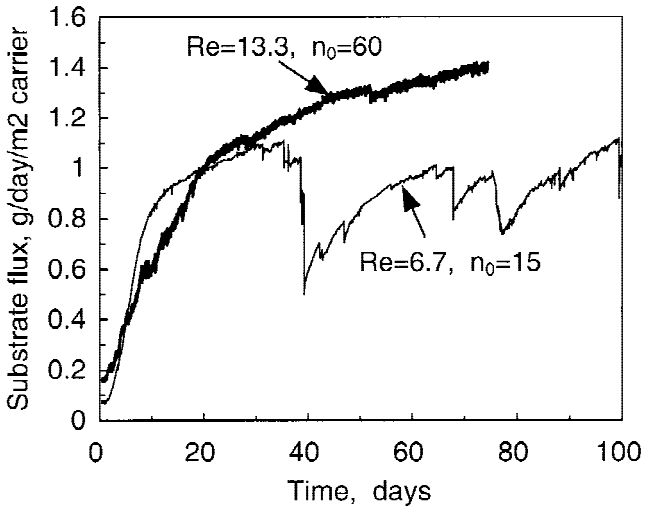

Figure 6. Variation in time of calculated substrate flux per carrier unit area (in gm^{-2} day^{-1}) at G = 562, Re = 13.3, σ_t = 0.4 N m^{-2}, n_0 = 60 grid cells inoculated (corresponds to case d in Table II, and Fig. 5a–5e) and at G = 562, Re = 6.7, σ_t = 0.4 N m^{-2}, n_0 = 15 grid cells inoculated (corresponds to case a in Table II, and Fig. 5f–5j).

growing biofilms was found in detachment experiments by Tijhuis et al. (1995), Gjaltema et al. (1995), and Villaseñor et al. (1999). In these studies, when the nutrient supply was stopped, the detachment rate decreased asymptotically to very low values in a few hours. This supports the hypothesis of a biofilm "mechanical steady state," where in the absence of growth, the biofilm structure is eroded such that it does not easily permit further detachment (at least in shortterm experiments).

At high substrate concentration (low G), the biofilm breaks when it reaches a higher thickness (130 μm compared with 60 μm), and sloughing starts earlier (after only 6 days instead of 30 days). Also, the average biofilm thickness and the biomass accumulated on carrier in the sloughing phase are bigger at low than at high G. Although the biofilm developed faster and thicker at high substrate concentration, its formation was characterized by a higher instability than at low concentration (compare biomass accumulation curves in Fig. 2a with 2c, and in Fig. 2d with 2f). Periods of sharp and unlimited growth alternated with abrupt biomass loss (Fig. 2c). Moreover, at G = 562 and Re = 13.3 a stable state in biofilm accumulation and biofilm thickness was reached, which did not happen in any of the other studied cases.

Re Number

The flow regime has a double influence on biofilm formation. As expected, at higher flow velocities the substrate flux towards the biofilm is increased by the diminished external resistance in the boundary layer. This intensifies the biofilm growth rate in the mass-transfer-limited regime, while the exponential phase is still the same. On the other hand, high Re means a high shear stress at the biofilm surface. This generates a greater detachment rate, as can be seen in Table II (compare $\overline{\Phi}_{X,d}$ in case (a) with (d), (b) with (e), and (c) with (f), respectively). In the "only erosion" regime, the percentage of detached biomass from the newly grown biofilm was always several times bigger at the higher flow rates.

At Re = 13.3, the biofilms remained thin, both averaged over the sloughing stage and also when the first important breakage occurred. These results are very normal, because the higher the Re, the stronger the forces that the biofilm structure must withstand. Also, the sloughing events started earlier for the higher Re regime at a cohesion strength of σ_t = 1 Nm^{-2}. However, at σ_t = 0.4 Nm^{-2} there was a much later sloughing (case f in Table II) or none at all (case d). Although at first sight this appears paradoxical, this can be explained by the fact that continuous erosion shaped a more compact, and thus mechanically more stable biofilm (see Fig. 5). Hence, the causes for sloughing must be sought not only in the biofilm strength, but also in its shape.

Cohesion Strength

The effect of biofilm cohesion strength σ_t can be examined by comparing simulation (a) with (b) and (d) with (e) in Table II. Basically, an increase in biofilm strength has the same effect on the biofilm detachment rate as does a lower Re, namely less detachment. During the mass-transfer-limited growth phase, the stronger biofilm suffers almost no erosion at Re = 6.7 (Table II, case b). It is interesting, however, that in the erosion phase, the biomass growth rate also diminished in mechanically stronger biofilms. Again, this seems to be a contradictory prediction, but a plausible explanation exists. From Table II we can see that stronger biofilms develop a structure with a more irregular surface. According to the mass transfer model presented in Picioreanu et al. (2000a), substrate mass transfer rate to rougher biofilms is smaller. The immediate result is a lower biomass growth rate.

The sloughing phase starts later for stronger biofilms. More biomass must accumulate on the carrier before massive breakage can occur. Also, the amount of biomass on the carrier averaged through the sloughing phase is larger (for example, the dashed line on Fig. 2a is at 0.24 g/m^2 compared with 0.31 g/m^2 in Fig. 2b for the stronger biofilm). Because stronger biofilms resist higher liquid forces applied on their surface, they can grow thicker (75 μm compared with 55 μm at Re = 6.7, and 65 μm compared with 25 μm at Re = 13.3).

Ohashi et al. (1999) points to the fact that, in wastewater-treatment reactors, shear stress acting on the biofilm surface is generally below 1 N/m^2. This value is smaller than the tensile strength recently measured by Ohashi et al. (1999), which suggests that fluid shear is not likely to produce massive biofilm erosion. An alternative mechanism for detachment could be due to cavity formation inside the biofilm, due to biomass decay. This mechanism is supported by the determined relationship between tensile strength and the dry density. In experiments by Ohashi et al. (1999), the ultimate tensile strength increased with an increasing dry density. If cells are decaying in the biofilm depth, due to aging or starvation, then cavities can be formed at the carrier-biofilm interface (Ohashi and Harada, 1994, 1996). A 10–20% cavity area caused a drastic decline of cohesion strength, followed by massive biofilm detachment. These observations can be expected to result from our mathematical model by defining the mechanical properties of biomass contained in each finite element (such as elastic modulus, cohesion strength, or tensile strength), as a function of cell and EPS content.

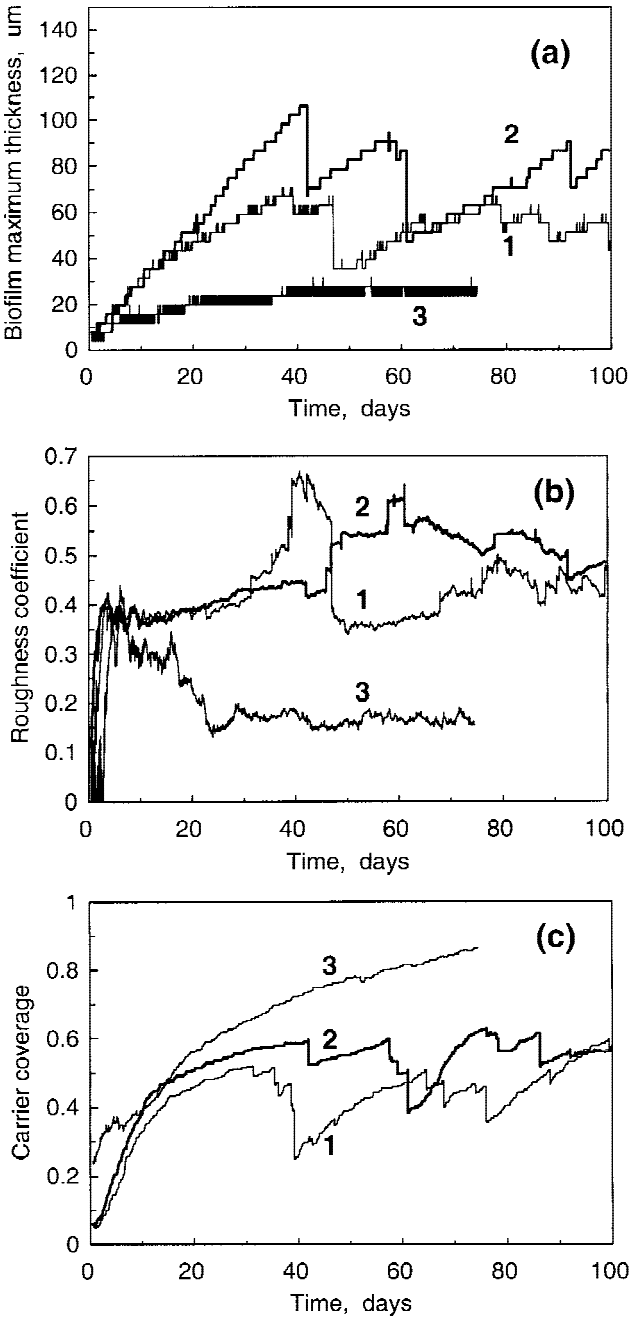

Figure 7. Variation in time of (a) biofilm maximum thickness achieved (in μm), (b) coefficient of roughness for the biofilm-liquid interface, (c) carrier surface coverage. Numbers on the graphs indicate simulation results at: (1) G = 562, Re = 6.7, σ_t = 0.4, (2) G = 562, Re = 6.7, σ_t = 1, (3) G = 562, Re = 13.3, σ_t = 0.4.

Biofilm Structural Properties

Several biofilm structural properties, as they evolve in time, are presented in Figure 7. Due to the massive removal of biofilm at certain stages, the curves of the biofilm maximum thickness, coefficient of surface roughness, and carrier coverage in time now have a more fluctuating appearance. By studying Figure 7b, it becomes clear that surface roughness increases considerably after massive detachment events (visible from the biofilm thickness graphs in Fig. 7a). It can also be noticed that the compact biofilm formed at G = 28, Re = 13.3 and σ_t = 0.4 N m^{-2} has not only the lowest average roughness coefficient (0.16), but it is also the thinnest film of the six simulated (25–30 μm, see Fig. 7a and Fig. 6). Also, the carrier surface coverage reached almost 90% (Fig. 7c).

Mushroom-Like Colonies

Unexpectedly, in some biofilm breaking stages, mushroom structures very similar to those reported in Lewandowski et al. (1995) appeared (see Fig. 3j). The simulation results from our model seem to show that there could be more than one possible physical mechanism for occurrence of the "mushroom" structures reported repeatedly in the literature:

1. Nutrient depletion leads to a competition between colonies separated by small distances. In the initial stages, when plenty of nutrient is available, they all grow in favorable conditions. Due to their uneven distribution on the carrier surface, some colonies will get more substrate, will grow faster and will dominate the others. Later, these dominating colonies will spread faster at the top, covering more volume than in the initial phase. This mechanism also implies the existence of other dominated colonies in the neighborhood that exhibit exactly the opposite tendency: to narrow their peaks in a conic shape.
2. Breaking of "tower-like" biofilm formations occurs most often at their base, near the attachment interface with the substratum. This is, on one hand, due to the fact that most deformation stress is concentrated there, but also because decaying processes and cavity formation especially weaken those deep areas. If patches break from the base of a cylindrical or hemispherical colony, a "mushroom-like" structure can be formed. This is clearly shown in Fig. 3i–j. If cohesion strength is represented in the model as a function of cell content (as indicated by Ohashi's work), then more "mushroom-like" biofilm clusters are expected to develop.

Distribution of Detached Biomass

Stewart (1993) pointed out that in many biofilm systems there is a broad distribution of detached particle sizes. Sometimes, this makes it difficult to clearly say when detachment is dominated by erosion or by sloughing. Simulation results of this model can be also analyzed from this perspective. We calculated the fraction of total biomass detached due to detached particles with a certain mass. Distribution of this fraction as a function of detached particle mass is plotted in Figure 8. When G = 562, Re = 13.3, and σ_t = 0.4 N/m^2 (case d in Table II), 90% of the total detached biomass came from particles with ρ_x below 0.003 g/m^{-2}. Conversely, when G = 562, Re = 6.7, and σ_t = 1 N/m^2 (case b in Table II), 92% of the total detached biomass came from particles with mass ρ_x greater than 0.01 g/m^{-2}. These data clearly show that in case (d) of biofilm growth, erosion was the dominating detachment mechanism, while in case (b), sloughing was mainly responsible for biomass loss.

Initial Colonization: Effect of Carrier Roughness

At $u_{X,max}$ = 0.02 m/s, the biofilm developed on the flat surface only for the higher cohesion strength (1 N/m^2).

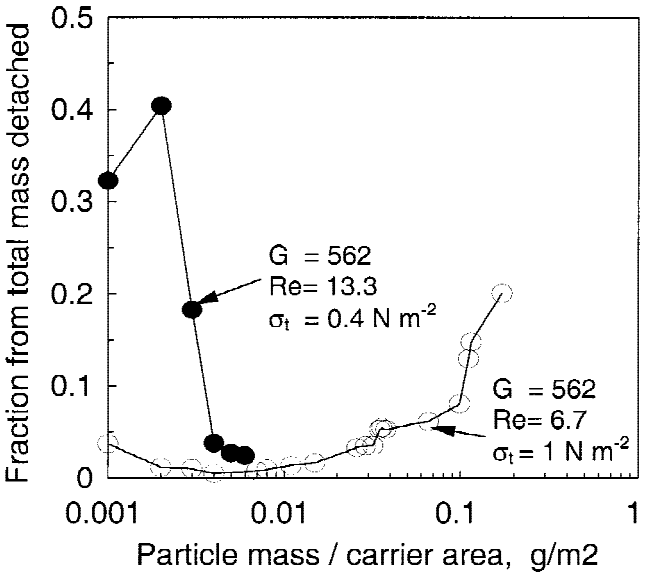

Figure 8. Distribution of detached particle mass (per carrier area) shows that sloughing is the main detachment mechanism at G = 562, Re = 6.7, and σ_t = 1 N m^{-2} (○; case b in Table II and Fig. 3); by contrast, erosion dominates at G = 562, Re = 13.3, and σ_t = 0.4 N m^{-2} (●; case d in Table II and Fig. 5a–5e).

When an cohesion strength of σ_t = 0.4 N/m^2 was set, all the colonizing cells were detached from the carrier surface in about 2–3 days. Biofilm accumulation is governed by the balance between processes leading to an increased amount of attached biomass, like microbial growth and cell adhesion, and those resulting in biomass loss, like detachment (Bryers and Characklis, 1982). To remain attached and to form a biofilm, either the detachment rate must be decreased, or the growth or attachment rates must be increased. Geometrical characteristics of the carrier surface are important because its roughness promotes bacterial colonization (Gjaltema et al., 1997; Van Loosdrecht et al., 1987; Verran et al., 1991). Fox et al. (1990) observed that carrier surface roughness was critical to biofilm development during the start-up period of an expanded-bed reactor. They hypothesized that biofilm growth begins in the crevices where protection from shear forces exists. As biofilm fills in the crevices, cell clusters from neighboring crevices join together, and a mature biofilm completely covers the rough surface.

To study the effect of carrier-surface texture on biofilm formation, the above conditions in which the simulated biofilm failed to develop were set (G = 526), but an irregular carrier surface was created. From the 15 colonies seeded, only 7 resisted detachment after 2 days (Fig. 9a). Sheltered in the carrier valleys, they developed a patchy biofilm. Finally, the biofilm entered a steady state, with all the newly formed biomass being sheared off by the liquid (Fig. 9c,d). The clusters completely filled the cavity in which they started to grow, but they were unable to further colonize the substratum. Any attempt to accumulate more biofilm resulted in its exposure to high-shear stress, which produced

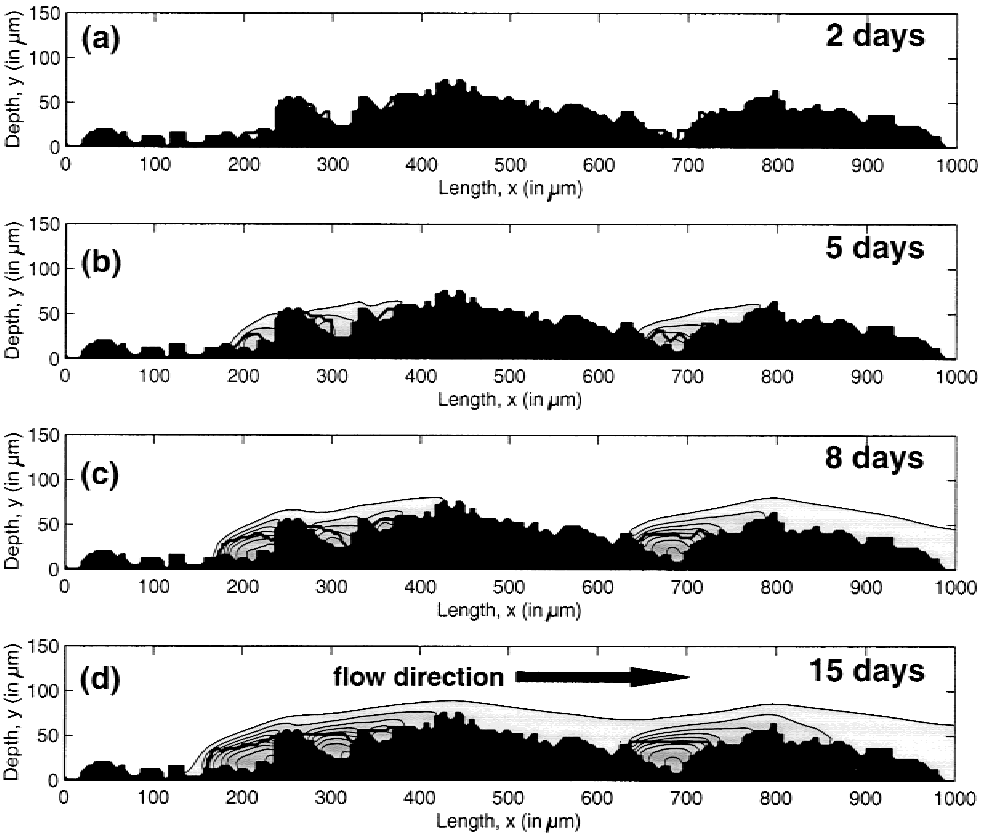

Figure 9. Simulated biofilm development on a rough carrier (substratum). Signification of lines and gray scale is as described in Figure 3. The black area is the carrier irregular relief. Flow direction is from left to right.

a high loss rate. The only mechanism that could lead to a colonization of neighboring valleys is reattachment, because none of the existing colonies is able to spill biomass over the carrier peaks. This numerical experiment reveals once again the necessity to introduce processes of cell attachment and reattachment in the model.

CONCLUSIONS

1. A two-dimensional model for detachment, based on internal stress created by moving liquid past the biofilm, is able to generate a variety of biofilm formation patterns. Two biofilm detachment mechanisms, erosion and sloughing, are modeled in a unified way. In the model, both are caused by stress developed in the biofilm structure. By plotting the distribution of the fraction from total biomass detached as a function of detached particle mass, which of the two mechanisms is dominant in the modeled biofilm system can be discriminated. This process can be experimentally evaluated by measuring the particle-size distribution in time (e.g., with an automated image-analyzing system connected to the outlet of a plug-flow biofilm reactor—like the flow-cell).
2. Model simulations showed that erosion (removal of small biofilm particles) makes the biofilm surface smoother. Sloughing (loss of large biofilm patches), by contrast, leads to an increased biofilm-surface roughness.
3. An avalanche effect in biomass loss was observed several times. Breakage of some biofilm structures left other colonies highly exposed to strong liquid shear. When these break, others will follow, leading to massive sloughing in a short period of time. This model behavior is in complete accordance with Stoodley's suggestion that "some sloughing events are triggered" when "the surface cover is reduced by the detachment of a few cell clusters" and, as a result, increasing drag on neighboring downstream clusters may then cause them to detach too." (Stoodley et al., 1999b).
4. Faster growing biofilms have a faster detachment rate then slow-growing biofilms, under similar hydrodynamic conditions. This is in agreement with the experimental evidence showing that detachment is dependent on both shear and growth rates.
5. High-growth rates trigger instability in biofilm accumulation and abrupt biomass loss. In our model, this happened especially at low G numbers, when the nutrient supply was high enough to support a fast growth of biomass. The causes for sloughing must be sought, not only in the biofilm strength, but also in its shape. Massive sloughing can be avoided by high liquid shear, combined with low biomass growth rates. This fact was also

experimentally observed in the biofilm-airlift reactor, when slow-growing microorganisms like nitrifiers formed much stronger and more compact biofilms than fast-growing heterotrophic populations.

6. Simulation results show that occurrence of the "mushroom-like" biofilm structures can be due to a combined effect of nutrient depletion and breaking at the colony base.
7. A rough carrier surface promotes biofilm development in hydrodynamic conditions in which the biofilm on a flat surface would not form. Although biofilm patches completely filled the cavity in which they started to grow, they were unable to spill over the carrier peaks and to further colonize pits in the carrier. This numerical experiment reveals the necessity to introduce in the model processes of cell attachment and reattachment. Implementation of these new processes is expected to increase the surface of the covered carrier, not only for the rough carrier, but also for the flat one after major sloughing events. However, the general trends discussed in this article will not significantly change.

APPENDIX

Equations of Plane Strain Problem

The plane strain approximation serves to represent a 3-D mechanical problem by a 2-D one if one considers a prismatic body whose length in z direction is large compared with its cross-sectional dimensions (in xy plane), and if the body is loaded uniformly along its length.

The equilibrium equations for a small element of material are (e.g., Benham et al., 1996):

$$\frac{\partial \sigma_x}{\partial x} + \frac{\partial \tau_{YX}}{\partial y} = 0 \qquad \text{(A1)}$$

$$\frac{\partial \sigma_Y}{\partial y} + \frac{\partial \tau_{YX}}{\partial x} = 0 \qquad \text{(A2)}$$

where the body forces (e.g., weight) were neglected—they were too small in comparison with the applied forces.

Because the two equations above contain three unknown stresses, the compatibility equation

$$\left(\frac{\partial^2}{\partial x^2} + \frac{\partial^2}{\partial y^2}\right)(\sigma_X + \sigma_y) = 0 \qquad \text{(A3)}$$

completes the set. The compatibility Equation (A3) is derived by considering the stress-strain physical equations applied for the plane-strain case:

$$\varepsilon_X = \frac{1+\nu_P}{E}[\sigma_X - \nu_P(\sigma_X + \sigma_y)]$$

$$\varepsilon_Y = \frac{1+\nu_P}{E}[\sigma_Y - \nu_P(\sigma_X + \sigma_y)]$$

$$\gamma_{YX} = \frac{2(1+\nu_P)}{E}\tau_{YX}$$

It was also considered that the internal stress exerted by growing cells in the gel matrix is negligible, and affects neither of the strain components (ε_X, ε_Y, γ_{YX}).

Because Equations (A1)–(A3) are applied here for a stress-boundary problem, stress components at the biofilm–liquid interface are specified, as they result from solution of Navier-Stokes equations. On the biofilm-carrier interface zero-displacement condition is set, i.e., the biofilm cannot migrate on the carrier surface.

All the simulations were performed on the Cray T3E of the Center for High Performance Applied Computing in Technical University Delft.

References

Applegate DH, Bryers JD. 1990. Bacterial biofilm sloughing. Nutrient limitation effects. In: Bont JAM, Visser J, Mattiasson B, Tramper J, editors. Physiology of immobilized cells. Amsterdam: Elsevier. p 87.

Benham PP, Crawford RJ, Armstrong CG. 1996. Mechanics of engineering materials. Harlow, Essex, UK: Longman Grp Ltd.

Bishop P, Rittmann BE. 1996. Modelling heterogeneity in biofilms: Report of the discussion session. Water Sci Technol 32(8):263–265.

Bryers JD, Characklis WG. 1982. Processes governing primary biofilm formation. Biotechnol Bioeng 24:2451–2476.

Bryers JD. 1988. Modeling biofilm accumulation. In: Bazin MJ, Prosser JI, editors. Physiological models in microbiology, vol. 2. Boca Raton, FL: CRC Press. p 109–144.

Chen S, Dawson SP, Doolen GD, Janecky DR, Lawniczak A. 1995. Lattice methods and their applications to reacting systems. Comp Chem Eng 19(6/7):617–646.

Christensen BE, Characklis WG. 1990. Physical and chemical properties of biofilms. In: Characklis WG, Marshall KC, editors. Biofilms. New York: John Wiley & Sons. p 93–130.

Eberl H, Picioreanu C, van Loosdrecht MCM. 1999. Modelling geometrical heterogeneity in biofilms. Proceedings of The 13th International Conference of High Performance Computing Systems & Applications, June 1999, Kingston, Canada. In: Pollard A, Mewhort DJK, Weaver DF, Eds. Kluwer Academic Press. p 497–512.

Fox P, Suidan MT, Bandy JT. 1990. A comparison of media types in acetate fed expanded-bed anaerobic reactors. Water Res 24(7): 827–835.

Gjaltema A, Arts PAM, van Loosdrecht MCM, Kuenen JG, Heijnen JJ. 1994. Heterogeneity of biofilms in rotating annular reactors: Occurrence, structure and consequences. Biotechnol Bioeng 44:194–204.

Gjaltema A, Tijhuis L, van Loosdrecht MCM, Heijnen JJ. 1995. Detachment of biomass from suspended nongrowing spherical biofilms in airlift reactors. Biotechnol Bioeng 46:258–269.

Gjaltema A, van der Marel N, van Loosdrecht MCM, Heijnen JJ. 1997. Adhesion and biofilm development on suspended carriers in airlift reactors: Hydrodynamic conditions versus surface characteristics. Biotechnol Bioeng 55:880–889.

Hermanowicz SW. 1998. A model of two-dimensional biofilm morphology. Water Sci Tech 37:219–222.

Hibbeler RC. 1991. Mechanics of materials. New York: Macmillan.

Hinton E, Owen DRJ. 1977. Finite element programming. London: Academic Press.

Lewandowski Z, Stoodley P, Altobelli S. 1995. Experimental and conceptual studies on mass transport in biofilms. Water Sci Technol 31(1): 153–162.

Ohashi A, Harada H. 1994. Adhesion strength of biofilm developed in an attached growth reactor. Water Sci Technol 29(10–11):281–288.

Ohashi A, Harada H. 1996. A novel concept for evaluation of biofilm adhesion strength by applying tensile force and shear force. Water Sci Technol 34(5–6):201–211.

Ohashi A, Koyama T, Syutsubo K, Harada H. 1999. A novel method for

evaluation of biofilm tensile strength resisting erosion. Water Sci Technol 39(7):261–268.
Picioreanu C, van Loosdrecht MCM. Heijnen JJ. 1998. Mathematical modeling of biofilm structure with a hybrid differential-discrete cellular automaton approach. Biotechnol Bioeng 58(1):101–116.
Picioreanu C, van Loosdrecht MCM, Heijnen JJ. 1999. Discrete—differential modelling of biofilm structure. Water Sci Technol 39(7): 115–122.
Picioreanu C. 1999. Multidimensional modeling of biofilm structure. Ph.D. thesis, Delft University of Technology, The Netherlands.
Picioreanu C, van Loosdrecht MCM, Heijnen JJ, 2000a. A theoretical study on the effect of surface roughness on mass transport and transformation in biofilms. Biotechnol Bioeng 68(4):355–369.
Picioreanu C, van Loosdrecht MCM, Heijnen JJ. 2000b. Effect of diffusive and convective substrate transport on biofilm structure formation: A 2-D modeling study. Biotechnol Bioeng 69(5):504–515.
Rittmann BE. 1982. The effect of shear stress on biofilm loss rate. Biotechnol Bioeng 24:501–506.
Rittmann BE. 1989. Detachment from biofilms. In: Characklis WG, Wilderer PA, editors. Structure and function of biofilms. New York: John Wiley & Sons. p 49–58.
Stewart PS. 1993. A model of biofilm detachment. Biotechnol Bioeng 41(1):111–117.
Stoodley P, Lewandowski Z, Boyle JD, Lappin-Scott HM. 1998. Oscillation characteristics of biofilm streamers in turbulent flowing water as related to drag and pressure drop. Biotechnol Bioeng 57(5):536–544.
Stoodley P, Lewandowski Z, Boyle JD, Lappin-Scott HM. 1999a. Structural deformation of bacterial biofilms caused by short-term fluctuations in fluid shear: An in situ investigation of biofilm rheology. Biotechnol Bioeng 65:83–92.
Stoodley P, Boyle JD, De Beer D, Lappin-Scott HM. 1999b. Evolving perspectives of biofilm structure. Biofouling 14(1):75–90.
Tijhuis L, van Loosdrecht MCM, Heijnen JJ. 1995. Dynamics of biofilm detachment in biofilm airlift suspension reactors. Biotechnol Bioeng 45:481–487.
Tijhuis L, Hijman B, van Loosdrecht MCM, Heijnen JJ. 1996. Influence of detachment, substrate loading and reactor scale on the formation of biofilms in airlift reactors. Appl Microbiol Biotechnol 45:7–17.
Van Loosdrecht MCM, Lyklema J, Norde W, Schraa G, Zehnder AJB. 1987. Electrophoretic mobility and hydrophobicity as a measure to predict the initial steps of bacterial adhesion. Appl Environ Microbiol 53:1898–1901.
Van Loosdrecht MCM, Eikelboom D, Gjaltema A, Mulder A, Tijhuis L, Heijnen JJ. 1995. Biofilm structures. Water Sci Technol 32(8):35–43.
Van Loosdrecht MCM, Picioreanu C, Heijnen JJ. 1997. A more unifying hypothesis for the structure of microbial biofilms. FEMS Microb Ecol 24:181–183.
Verran J, Lees G, Shakespeare AP. 1991. The effect of surface roughness on the adhesion of *Candida albicans* to acrylic. Biofouling 3:183–192.
Villaseñor JC, van Loosdrecht MCM, Picioreanu C, Heijnen JJ. 1999. Influence of different substrates on the formation of biofilms in a biofilm airlift suspension reactor. In Proceedings of the 4th IAWQ Conference on Biofilm Systems, October 17–20, 1999, New York.
Wanner O, Gujer W. 1986. A multispecies biofilm model. Biotechnol Bioeng 28:314–328.
Wanner O, Reichert P. 1996. Mathematical modeling of mixed-culture biofilms. Biotechnol Bioeng 49:172–184.
Wimpenny JWT, Colasanti R. 1997. A unifying hypothesis for the structure of microbial biofilms based on cellular automaton models. FEMS Microb Ecol 22:1–16.